INTERNATIONAL JOURNAL OF ENGINEERING MANAGEMENT SCIENCE
journal homepage: www.ijems.online/index.php/ijems/index

DESIGN, IMPLEMENTATION AND VALIDATION OF EV POWERTRAIN AND SAFETY SYSTEMS

Akshay Gowda HK[1,*], Gopika P Prasad[2], Harika L T[3], Neel Mannuel Sebastian[4], Umavathi M[5], Rajesh P[6]

[1,2,3,4] Electrical and Electronics Engineering Department Students, BMSCE, Bangalore - 560019.
[5]Associate Professor, Electrical and Electronics Engineering Department, BMSCE, Bangalore - 560019.
[6]Associate Professor, Mechanical Engineering Department, BMSCE, Bangalore - 560019.
***Corresponding E-mail:** akshaygowda.ee22@bmsce.ac.in

Received: 5-4-2026 ***Revised: 15-5-2026*** ***Accepted: 31-5-2026***

Keyword
Electric Vehicle (EV), Lithium-Ion Accumulator, Precharge Circuit, Discharge Circuit, Brake System Plausibility Device (BSPD), High-Voltage Protection, Modular Battery Pack, Formula Student.

Abstract
For reliable energy storage in the mid-voltage EV powertrain, correct sizing of the cells alone is not enough. The accumulator system must provide dependable electrical output throughout all system operational states, which include system initiation, operation, and shutdown, especially during fault-related equipment failures. This paper describes the development and verification of a 96V class modular lithium-ion accumulator configured in the 18p24s arrangement providing 88.8V and 100.8V nominal and maximum voltages correspondingly, with an approximate total usable energy storage of 6.5kWh.

The busbar system consists of two materials, where nickel is used for connections in parallel, while aluminium is used for connections in series. Such a configuration ensures balanced currents at the 200A operational rating. There are three protection devices employed and verified: a pre-charge circuit preventing high inrush current to the motor controller; a passive discharge path, which decreases the DC-link bus voltage to under 10V after the relay disconnection; a hardware-based Brake System Plausibility Device (BSPD) that triggers the disconnection of isolation relays when both brake and throttle switches are activated simultaneously without requiring software implementation.

A 24s1p mini-accumulator was built to test its performance at the complete system voltage. This method prevented repeated fault tests on the entire 432-cell assembly. The precharge circuit needs about 3 seconds to reach 96 percent of the relay closure point according to the recorded data. The discharge circuit successfully reaches the 10 V requirement within the calculated time, while the BSPD functioned to the requirements completing relay isolation in less than one second. The analytical predictions are similar to the hardware measurements with high accuracy, which proves that lumped-parameter RC analysis is an effective method for designing protection circuits in the chosen voltage and capacitance range.

1. Introduction:

The connection of a high-voltage lithium-ion accumulator to a motor controller in a mid-voltage electric vehicle requires three protection methods which cannot be solved through cell sizing only. The system needs to manage inrush current during startup while the bus voltage must reach a secure threshold after isolation and the system needs to respond instantly to simultaneous brake and throttle activation. Each of these arises from a distinct failure mechanism and each demands a dedicated circuit before the system can be considered safe for operation or maintenance.

The inrush problem occurs at the interface between the accumulator and the DC-link capacitors of the motor controller. At startup, these capacitors are discharged. Direct closure of the main isolation relay connects the fully charged pack to what is, at that moment, a near-zero impedance load. The peak transient current reaches several hundred amperes which exceeds the steady-state design current and causes mechanical damage to contactor surfaces beyond their operational limit [1] The documented causes of contactor failure in high-voltage automotive systems show that repeated transient exposure leads to premature contactor failure [2].

The precharge resistor, which exists before the main relay, transforms the event into a controlled RC transient. The shutdown process creates a second danger, which matches the importance of the first danger. The DC-link capacitors store energy, which does not release when isolation relays open. The bus maintains nearly full pack voltage until it discharges for multiple minutes after disconnection without an active discharge path [3]. The relay state does not show this risk, which exists when maintenance personnel work with high-voltage connectors. The DC bus resistor operates without requiring any downstream load because it established a passive drain pathway. The rules for Formula Student competitions follow standard automotive functional safety requirements which classify simultaneous brake and throttle activation as a sensor failure or control inconsistency fault condition [4]. The Brake System Plausibility Device (BSPD) uses comparator logic to detect system conditions which trigger isolation relay openings without needing a software response path for the defined time window. The existing resources do not provide a unified approach that studies pack architecture together with all three protection subsystems, which were tested at full system voltage on a single platform [6]. This paper addresses that gap.

The 96 V class, 18p24s accumulator described here was designed for Formula Student competition. The protection architecture, however - RC precharge design, passive discharge sizing, and comparator-based BSPD logic, applies to any mid-voltage EV traction system in the 80 - 100 V range.

2. REVIEW OF LITERATURE

2.1 Lithium-Ion Cell Configuration and Parallel Group Behavior

The energy capacity requirements of a lithium-ion battery pack which uses series-parallel configuration show multiple effects on its performance. The researchers Bruen and Marco [5] used controlled cycling tests to establish that when one parallel group comprises two cells with 30% impedance difference, then the peak current distribution between those cells will show 60% variation which results in more than 6% charge changes during each testing cycle. As time progresses the battery cell conducting the highest electrical load will age faster which leads to greater current imbalance. The study results establish support for the multi-tab welding technique which this study uses to decrease interconnect resistance changes between cells at their connection points. Paudel et al. [9] demonstrated that modular pack segmentation helps in faster fault testing as technicians can identify damaged cell groups through their dedicated modules instead of needing to remove the entire system.

2.2 Precharge Circuit Design and Inrush Current Limitation

The three-state precharge sequence of negative contactor closure followed by resistor-limited charging and main contactor closure at near-pack voltage establishes standard procedures for preventing contactor damage through inrush current. The researchers discovered that closure threshold serves as the most important factor because closing too soon causes the current spike to occur during engagement instead of disappearing. Ozguc et al. [2] conducted SPICE simulation on a Tesla Model S system to compare resistor-based and MOSFET PWM precharge methods. The semiconductor method achieved better results because it reduced sequence time to 40 ms while peak switch dissipation reached 5.275 kW, which required separate thermal management to handle, compared to the resistor method that had 3.25 kW peak dissipation. The researchers concluded that the resistor-based approach provides superior simplicity and reliability for systems which need multi-second precharge time because it works directly with the 96 V 2.7 mF system described in this paper.

2.3 High-Voltage Isolation, Discharge, and Safety Architecture

The work carried out by Habib et al. [3] examined EV energy storage and protection architectures, which showed that DC-link capacitors maintain energy storage at pack voltage after the relay opens because the system lacks active discharge capabilities a maintenance risk which the passive discharge resistor approach solves through continuous power discharge at minimal expense. The researchers determined that resistance value selection creates a two-sided limitation because high values result in longer discharge periods while low values increase ongoing power use. West et al. [4] explained an FSAE Electric accumulator design which demonstrated that Formula Student rules directly influence hardware choices especially for relay selection because the contactor's inrush capacity limits the maximum voltage differential allowed during closure. Their work proved that using segmented modules leads to simpler verification processes, matching the six-module system design employed in this study.

2.4 EMI Considerations and Powertrain Integration

Kharanaq et al. [10] studied EMI modeling research which was conducted in motor drive systems and they found that startup switching transients produced the highest level of electromagnetic emissions. The precharge RC network reduces dV/dt during startup to establish two advantages which are not typical in precharge research because it protects contactor components and it decreases conducted emissions. Tonoli and Leotta [6] studied pack architecture through the lens of powertrain integration because they wanted to demonstrate that BMS voltage monitoring and relay closure readiness logic become easier with symmetric series sub-module designs. Xu et al. [7] found that EV traction systems experience increasing stress on isolation relay contacts because workers must repeatedly test the system in ways that exceed normal operational limits which justifies the use of a 96% closure threshold because it prevents secondary inrush events during all operational cycles.

3. LITERATURE GAP

Accumulator sizing, precharge design, and individual protection circuits each have documented design procedures in the literature. What is harder to find is a single platform where all three protection subsystems share a common set of design parameters, specifically the same DC-link capacitance, and are then validated together at full system voltage in hardware. Published Formula Student designs tend to focus on either the pack structure or the safety architecture, not both in one experimentally verified document. That is the gap this work addresses.

4. RESEARCH PURPOSE

The aim is to design and experimentally verify a 96 V class modular lithium-ion accumulator with three integrated protection circuits - precharge, discharge, and BSPD on a single platform. Beyond the Formula Student context, the architecture and sizing procedures documented here are intended as a usable reference for mid-voltage EV traction systems in the 80 - 100 V range, where this combination of pack design and protection sequencing is currently under-documented.

5. ACCUMULATOR DESIGN AND PROTECTION SYSTEM METHODOLOGY

5.1 System architecture

The high-voltage system is built around a modular 96 V class lithium-ion accumulator subdivided into six mechanically and electrically identical 4s18p modules. This segmentation reduces assembly to a set of repeatable units and allows each module to be tested in isolation before integration into the series chain — a practical advantage given that a faulty parallel group in a monolithic pack is difficult to locate without full disassembly. The six modules are joined in series through aluminium busbars to reach the target system voltage, while eighteen cylindrical cells within each module are connected in parallel through nickel strip interconnects. The overall architecture is shown in Fig. 1.

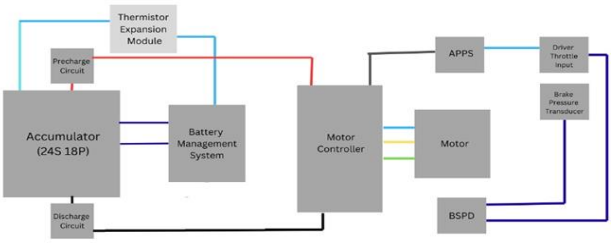

Figure 1: Overall high-voltage system architecture

The different interconnect materials used at cell and module levels are selected because each interface has specific requirements. Nickel enables effective resistance spot welding while it helps to maintain uniform current distribution throughout the cell terminals. Aluminium enables inter-module conductors to carry higher currents because it has lower electrical resistance and lighter weight than other materials. The two materials need to be kept in different functions because nickel operates at the cell interface while aluminium supports the series path, which prevents problems that arise from welding or bolting different materials together at high current levels.

The 18-cell parallel group uses multiple nickel tabs to connect each cell terminal instead of using a single strip. This method enables current distribution across multiple weld points, which helps to decrease resistive heating that occurs at each contact point. The series conductors and inter-module conductors use aluminium material, which has been designed to support 200 A of continuous operation. The choice of aluminium over copper reduces conductor mass at the cost of higher resistivity, at the cross-sectional areas required for 200 A, this is an acceptable trade-off for a weight-sensitive competition vehicle.

The motor controller connects to the accumulator through two main isolation relays. The system needs both relays to stay closed because opening any of them will separate the traction system from the power pack. The startup sequence system needs to be executed in multiple stages to control the power during system start-up, which includes:

- Precharge phase: A resistor is inserted in series with the positive rail. The motor controller's DC-link capacitors charge through an RC curve until they reach the voltage of the power pack.
- Main relay closure: When the DC bus reaches 96% of pack voltage the precharge resistor gets bypassed and the main relays close.
- Normal operation: The traction system receives full power from the pack voltage. The system requires complete power from the battery pack to deliver traction power. The isolation relays open during both commanded and fault-based shutdowns. The system uses the discharge resistor to drain capacitor charge until the voltage drops below 10 V which makes the system safe to handle. The BSPD operates continuously during traction. A fault output immediately opens the isolation relays and holds the system offline for 10 seconds before permitting automatic reset. The BSPD output connects directly to the relay coils which requires no software intervention.

5.2 Accumulator sizing methodology

Sizing the accumulator starts with voltage followed by energy and current - each step feeding into the next. The target was approximately 6.5 kWh at a nominal voltage near 96 V, with the pack capable of delivering 200 A continuously to the traction system.

A. Voltage and Configuration Selection

The number of cells in series is obtained by dividing the target maximum voltage by peak voltage of the selected cell. For cylindrical lithium-ion cells rated at 3.7 V nominal and 4.2 V peak:

$$V_{max} = N_s \times V_{peak(cell)} \quad (1)$$

$$96 = N_s \times 4.2$$

$$N_s \approx 22.85$$

A minimum of 23 series cells is required based on equation (1). Since, odd number of cells cannot be divided into identical sub-modules as it causes voltage imbalance across segments. It also complicates both balancing and voltage monitoring. Hence, using 24 cells resolves this issue allowing subdivision into six identical 4-series segments each having the same voltage at any given state of charge:

$$V_{max} = 4.2 \times 24 = 100.8 \text{ V}$$

$$V_{nom} = 3.7 \times 24 = 88.8 \text{ V}$$

The required 96 V is achieved by using 24 cells in series which has a margin of 4.2 V at nominal and a margin of 4.8 V at maximum relative to the minimum acceptable count.

B. Energy Requirement and Parallel Sizing

The pack energy required was calculated to be 6.5 kWh based on the energy consumed per lap and the target race distance. The relationship between parallel cell counts and pack energy is given by equation (2)

$$E_{pack} = N_p \times V_{nom} \times C_{cell} \quad (2)$$

Using $N_s = 24$, a nominal cell voltage of 3.7 V, and a cell capacity of 4.2 Ah:

$$E_{pack} = N_p \times 24 \times 3.7 \times 4.2$$

$$6500 = N_p \times 372.96$$

$$Np \approx 17.4$$

Since fractional cells are not practical and feasible, the required number of operational cells in parallel is finalised to 18 which acts as a safety net against voltage sag and capacity variation. Pack energy at this count works out to:

$$E\ pack = 18 \times 24 \times 3.7 \times 4.2 \approx 6.71\ kWh \quad (3)$$

Limiting the charging and discharging cycles to 80 to 90 percent of the theoretical capacity from equation (3), results in a usable energy that meets the 6.5 kWh target. The resulting 18p24s topology appears in Figure 2.

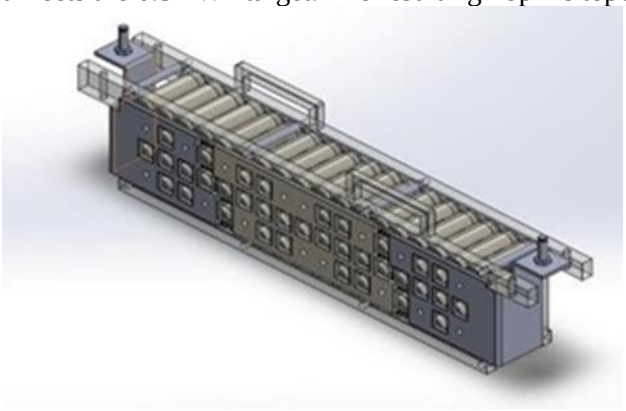

Figure 2: CAD representation of 18p4s modular accumulator segment

C. Current Handling Capability

Each cell has a continuous discharge rate of 45 A. So, the peak discharge current for the parallel group of cells is

$$I\ group(max) = 18 \times 45 = 810\ A \quad (4)$$

The rating of the motor controller and the fuse limit the traction current at 200 A. At that operating point, each cell carries:

$$Icell = 200 / 18 \approx 11.1\ A \quad (5)$$

The current operation of the system delivers 25 percent of the maximum per-cell current which equation (5) designates as the system's rated capacity. The operation of cells at this reduced level enables three benefits which include decreased internal resistance losses and maintenance of low voltage drop at pack terminals during load operation and slower capacity degradation compared to running the system at its maximum current. The available headroom allows busbar current density to operate below its maximum capacity which enables designers to select cross-section dimensions for interconnect materials using a more cautious approach.

D. Busbar Dimensioning

Aluminium series busbars were sized at 0.8 mm^2 per ampere of continuous current:

$$A = I \times 0.8\ mm^2/A \quad (6)$$

$$A = 200 \times 0.8 = 160\ mm^2$$

The 160 mm^2 cross-section from equation (6) maintains resistive power loss in control at 200 A while providing the busbar sufficient strength to withstand deformation. The 0.8 mm^2/A figure already incorporates a derating factor relative to the thermal limit of aluminium; the derated starting point provides adequate margin without needing to model steady-state temperature rise for every geometry variant.

Nickel tabs at the cell level follow the same logic: multiple tabs per terminal spread the 11.1 A per-cell current from equation (5) across several weld points which maintain low local resistive heating at each interface.

5.3 Protection and Safety Architecture

The protection architecture handles three failure modes through three independent solutions which include uncontrolled capacitive inrush at startup, hazardous residual DC bus voltage after isolation and unsafe simultaneous brake-throttle activation during traction. Each subsystem operates on a dedicated hardware path - a failure in one does not compromise the others.

A. Precharge Circuit

At startup, the motor controller's DC-link presents a 2.7 mF capacitive load to the pack terminals. Without a precharge resistor, direct relay closure drives a transient given by equation (7):

$$I\ inrush = V\ pack / R\ path \quad (7)$$

With harness resistance typically below 100 mΩ, peak inrush at 88.8 V nominal can reach several hundred amperes - well above both the rated inrush capacity of contactors in this voltage class and the 200 A operating design point. The precharge resistor converts this into a controlled exponential transient as shown in equation (8):

$$V\,c(t) = V\,pack \times (1 - e{-}t/RC) \quad (8)$$

Where R is the precharge resistance and C is the 2.7 mF DC-link capacitance. The closure threshold was set at 96% of pack voltage, leaving less than 4% - roughly 3.5 V at nominal - across the relay contacts at engagement. This differential is too small to produce a measurable capacitive re-charge event at closure, as the voltage in equation (8) approaches V pack asymptotically. The precharge interval was designed to reach this threshold in approximately 3 seconds for the 2.7 mF load.

B. Discharge Circuit

When isolation relays open, energy stored in the 2.7 mF DC-link capacitance remains on the bus. At 88.8 V, this stored energy is:

$$E = ½ \times C \times V^2 = ½ \times 2.7 \times 10{-}3 \times 88.8^2 \approx 10.6\ J \quad (9)$$

While 10.6 J is small relative to pack capacity, the voltage at which it is stored is the relevant hazard. Without a discharge path, the bus stays near pack voltage indefinitely after relay opening. The discharge resistor provides a passive drain governed by equation (10):

$$V(t) = V0 \times e{-}t/RC \quad (10)$$

Where V_0 is the bus voltage at relay opening. To get the bus voltage below 10V within the specified time window, the resistor value was selected accordingly.

The selection of the resistor value has two constraints:

- the discharge time constant establishes the upper resistance threshold, and
- Instantaneous power dissipation at full bus voltage and the start of the decay in equation (10) sets the lower limit through the resistor's peak power rating.

C. Brake System Plausibility Device (BSPD)

The brake system protection device monitors brake and accelerator signals through two comparators which use fixed input thresholds to assess their respective signals. The system uses an AND gate to combine outputs which generates a fault signal when both inputs exceed their threshold limits, preventing false trips from single sensor noise or brief overlapping transients during normal operation.

Upon fault detection:

I. The BSPD output de-energizes both isolation relay coils directly opening them within the relay's mechanical dropout time.
II. A latching timer holds the coils de-energized for 10 seconds, preventing re-engagement even if the fault signal clears instantaneously.
III. The system resets automatically after the hold period when the fault condition disappears.
IV. The 10-second hold prevents rapid relay cycling under an intermittent fault. The direct hardware path from comparator output to relay coil means the response does not depend on any microcontroller or software state.

D. Integrated Protection Sequence

Startup:

I. Precharge relay gets closed and the main relay remains open.
II. DC bus rises along the RC curve of equation (8).
III. At 96% of pack voltage, main relay closes and the precharge relay opens.
IV. Full pack voltage is delivered to the motor controller.

Shutdown or Fault:

I. Both isolation relays open immediately.
II. Discharge resistor begins draining the DC-link capacitors as per equation (13).

III. Bus decays below 10 V within the designed discharge interval.
IV. In BSPD-triggered events, the 10-second hold prevents relay re-closure until the timer expires and the fault has cleared.

At no point in this sequence is the DC bus left at an uncontrolled voltage: during startup it is ramped through the precharge circuit and during shutdown it is actively drained through the discharge resistor.

6. RESULTS

6.1 Experimental setup

Protection circuit validation at full system voltage requires a source that replicates the pack's voltage characteristics without subjecting the complete 18p configuration to repeated fault-injection cycles. A 24s1p mini-accumulator was built for this purpose, shown in Fig. 3. By retaining the 24-series cell count, the mini-pack produces the same open-circuit voltage as the full pack at any given state of charge. Reducing the parallel count to 1 limits capacity and energy available per test cycle - acceptable, since the protection circuits are voltage-driven rather than capacity-driven. This approach also avoids degrading the full pack's 432 cells through development testing, particularly for the BSPD tests which involve deliberate relay dropout under load.

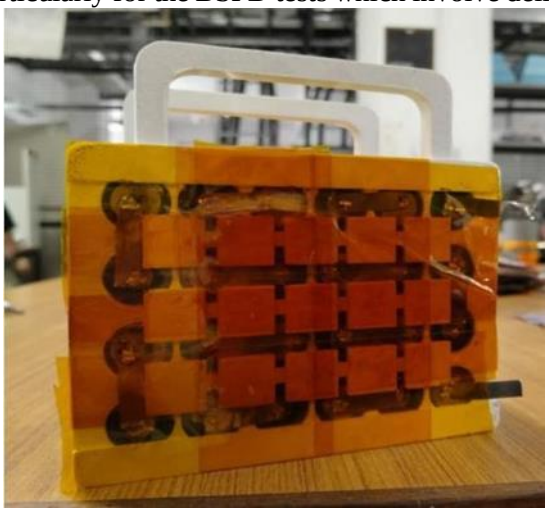

Figure 3: Fabricated 24s1p mini-accumulator used for experimental validation.

During validation, the mini-accumulator measured approximately 84 V — slightly below nominal due to partial discharge at the time of testing. The motor controller used across all tests presented a DC-link capacitance of 2.7 mF.

6.2 Precharge validation

DC bus voltage during startup was recorded using a digital storage oscilloscope (DSO) at 200 ms/div. The measured waveform followed the theoretical RC charging response of equation (8), as shown in Fig. 4.

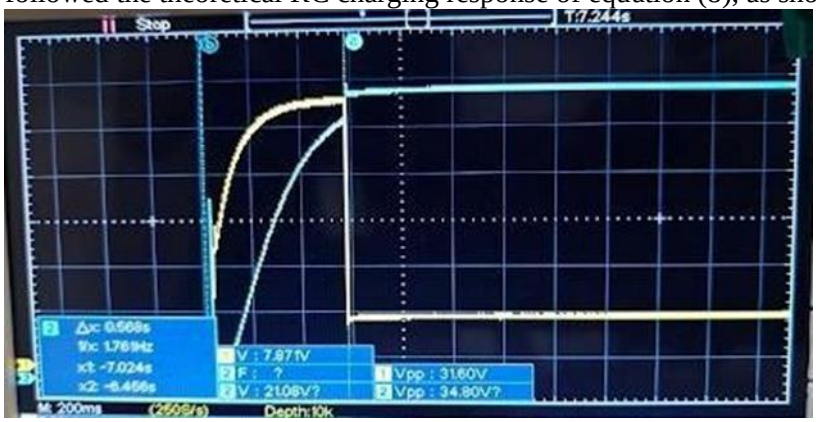

Figure 4: Experimental precharge waveform (200 ms/div) showing exponential DC bus voltage rise toward 84 V pack level.

The bus reached the 96% relay closure threshold:

$$V_{threshold} = 0.96 \times 84 \approx 80.6\ V \quad (14)$$

in approximately 3 seconds. The approach to threshold was monotonic with no oscillation or overshoot. At relay closure, no secondary current transient was detectable in the voltage waveform.

6.3 Discharge validation

Following relay opening, the discharge resistor was engaged and DC bus voltage decay was recorded. The bus voltage dropped below 10 V within the designed discharge interval.

6.4 BSPD functionality testing

The brake and throttle inputs received simultaneous signals which exceeded the BSPD comparator thresholds to create fault conditions, which were tested using a bench signal generator. The testing process separates from actual pedal hardware because it enables operators to inject faults at predetermined signal strength throughout the entire testing period.

The system measured relay dropout from the initial moment when the fault signal became active. Isolation was achieved during all test runs within a time period that lasted less than one second. There were no delayed dropouts or failures to detect faults. The system maintained an offline state for 10 seconds after each dropout until the automatic reset function activated. All testing procedures showed no signs of relay chatter during the hold period which occurred across multiple testing runs.

6.5 Summary of results

Table 1: Summary of analytical and experimental results

Parameter	Analytical Expectation	Measured Value	Observation
Pack Voltage (Test)	~88.8 V nominal	~84 V	Slight discharge during testing
Precharge Threshold	96% of pack voltage	~80.6 V	Relay closure verified at threshold
Precharge Duration	~3s (RC based)	~3s	Strong correlation with RC model
DC-Link Capacitance	2.7 mF	2.7 mF	Verified
Discharge Target	<10 V	<10 V	Achieved within safe interval
BSPD Isolation Time	<1s	<1s	Sub-second relay dropout
BSPD Reset Delay	10s	10s	Stable automatic reset

Table 1 summarizes design predictions and measured values across all three subsystems.

7. DISCUSSION

7.1 Precharge performance

The 3-second precharge time measurement for the 2.7 mF DC-link load matches with the time constant derived from equation (8). The lumped-parameter RC model functions as the suitable basis for precharge design work within this specific voltage and capacitance range. The work done by Ozguc et al. [2] support this conclusion because their SPICE simulations of the conventional resistor-based precharge sequence demonstrated that RC time-constant calculations accurately predict charging behavior when the main impedance path consists of the precharge resistance itself, which exists here because harness resistance remains below the precharge resistor value.

The relay closure test shows that 96% threshold selection successfully validates through its ability to detect secondary transient events. The test voltage of 84 V creates sufficient contact pressure. The precharge design process depends on the closure threshold as the key element according to Chang and Chen [8], who discovered that early closing merely shifts the inrush occurrence to the moment of engagement. The results here confirm that 96% eliminates this event without meaningfully extending the precharge interval. The long-term reliability

indicator for a system that undergoes multiple energization cycles during a competition season requires evaluation of inrush stress behavior at all closure points instead of relying on total events shown during bench tests.

7.2 Discharge behavior

The smooth exponential decay to below 10 V confirms two things: The actual discharge time constant of the built system matches the design intent which is described by equation (10) and the resistor maintained normal operation without reaching thermal derating during the test. The resistor would display a slower discharge rate when it reaches thermal limits because its resistance increases with temperature yet no such change appeared in the test results. Experimental confirmation of this point holds particular significance because the peak instant power dissipation takes place at the beginning of the event when the bus operates at full voltage which creates the most difficulty for assessment through steady-state thermal analysis.

7.3 BSPD functional robustness

Sub-second relay dropout across all fault injection trials confirms that BSPD response time is governed by the relay's mechanical dropout time rather than any latency in the detection logic. The stable 10-second hold across repeated trials confirms the timer implementation is not sensitive to fault signal state during the hold period - the condition that causes premature reset in a poorly designed latch. The direct hardware path from comparator output to relay coil, with no software in the loop, is the correct implementation for this class of safety function. West et al. [4] documented the same architectural requirement in their FSAE accumulator design, noting that hardware safety functions must remain independent of BMS software state to satisfy competition rules - a requirement that the present implementation meets.

8. CONCLUSION

This study set out to design and experimentally validate a 96 V class modular lithium-ion accumulator with three integrated hardware protection circuits - precharge, passive discharge, and BSPD on a single platform. Each of the five objectives stated at the outset was addressed and verified in hardware. The 18p24s topology arrived at through sequential sizing delivers 88.8 V nominal and 6.71 kWh theoretical energy capacity, with approximately 6.5 kWh available under practical state-of-charge limits. Operating the pack at 200 A continuous keeps per-cell current at 11.1 A, roughly 25% of the rated per-cell limit, providing substantial margin on both electrical and thermal stress. The dual-material busbar architecture, nickel at the cell interface and aluminium in the series path, distributes current uniformly across the 18-cell parallel groups. The finalised assembly, with six modular segments arranged within the enclosure, is shown in Fig. 5.

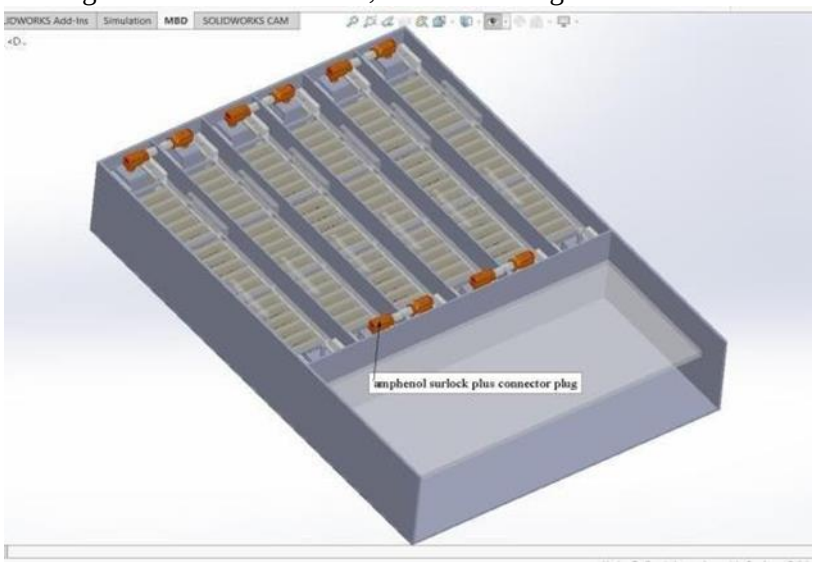

Figure 5: CAD model of the final 18p24s accumulator assembly having six modules within the enclosure with Amphenol Surlock Plus connectors.

The precharge circuit reached its 96% relay closure threshold after 3 seconds when testing with a 2.7 mF DC-link load which matched the RC model prediction and produced an unblemished relay closure without any secondary transient. The discharge circuit operation led to the DC bus voltage reducing to 10 V during the designated time period because the resistor maintained its power limits throughout the test based on the system's

gradual exponential voltage decrease. The BSPD achieved sub-second relay isolation across all fault injection trials, with a stable 10-second hold and clean auto-reset on every run. The measured behavior of all three subsystems matched analytical predictions sufficiently to demonstrate that lumped-parameter RC analysis serves as an effective design method for protection circuit sizing at this voltage and capacitance level.

The primary limitation of this work is that validation was conducted on a 24s1p mini-accumulator at approximately 84 V, slightly below the 88.8 V nominal due to partial discharge at the time of testing. The testing results better define protection circuits, which operate as voltage-driven systems while maintaining their valid RC model results through testing at full nominal and maximum pack voltage. The assessment of the discharge resistor's thermal behavior used decay profile smoothness to measure its thermal behavior and direct temperature measurement was not used - actual thermal testing needs to be done for worst-case scenarios which involve multiple discharge cycles at high ambient temperatures.

Future work should address long-term contactor reliability under repeated precharge cycles, discharge resistor thermal behavior under worst-case bus voltage and ambient conditions, and protection circuit performance under the dynamic load conditions present during actual on-track operation. Integrating an Insulation Monitoring Device and a Battery Management System into the same validated hardware platform would complete the safety architecture for full competition deployment. The design procedures and measured results documented here provide a consolidated reference for Formula Student teams and engineers working on mid-voltage EV traction systems where this combination of pack architecture and protection sequencing is currently under documented.

9. ACKNOWLEDGEMENT

The authors would like to express sincere gratitude to Dr. Umavathi M and Dr. Rajesh P for their guidance, feedback, and support throughout the duration of this project. Their inputs were valuable in shaping the direction of this work. The authors also thank BMS College of Engineering, Bangalore, for providing the laboratory facilities and equipment necessary to carry out the design, fabrication, and testing described in this paper. The support of the Research and Development department, BMS College of Engineering, is also acknowledged. No external grants or funding were received in support of this research.

10. CONFLICTS OF INTEREST

The authors declared no potential conflicts of interest with respect to the research, authorship, and/or publication of this article.

11. PLAGIARISM POLICY

All authors declare that any violation of plagiarism, copyright, or ethical matters is the responsibility of the authors. The journal and its editors bear no liability for such matters.

12. SOURCES OF FUNDING

No external funding was received to carry out this research work. All design and testing work was carried out using facilities at BMS College of Engineering, Bangalore.

References:

[1] Damodaran, V., Paramadayalan, T., Natarajan, D., Kumar C, R., Kanna, P.R., Taler, D., Sobota, T., Taler, J., Szymkiewicz, M. and Ahamed, M.J., 2024. Development of a fast running equivalent circuit model with thermal predictions for battery management applications. Batteries, 10(6), p.215. https://doi.org/10.3390/batteries10060215

[2] Ozguc, M.K., Ipek, E., Aras, K. and Erhan, K., 2019. Comprehensive analysis of pre-charge sequence in automotive battery systems. Transactions on Environment and Electrical Engineering, 4(1), p.1. https://doi.org/10.22149/teee.v4i1.136

[3] Habib, A.K.M.A., Hasan, M.K., Mahmud, M., Motakabber, S.M.A., Ibrahimya, M.I. and Islam, S., 2021. A review: Energy storage system and balancing circuits for electric vehicle application. IET Power Electronics, 14(1), pp.1–13. https://doi.org/10.1049/pel2.12013

[4] West, L., Shepherd, B., Karabon, N., Howell, J. and Pyrtko, M., 2016. Design report of the high voltage battery pack for Formula SAE Electric. Department of Mechanical Engineering, University of Wisconsin-Madison.

[5] Bruen, T. and Marco, J., 2016. Modelling and experimental evaluation of parallel connected lithium-ion cells for an electric vehicle battery system. Journal of Power Sources, 310, pp.91–101. https://doi.org/10.1016/j.jpowsour.2016.01.001

[6] Tonoli, A. and Leotta, F., n.d. Design of a battery pack for a Formula SAE racing car. [Unpublished manuscript].

[7] Xu, Y., et al., 2024. Improving powertrain efficiency through torque modulation techniques in single and dual motor electric vehicles. Transportation Engineering, 18, p.100289. https://doi.org/10.1016/j.treng.2024.100289

[8] Chang, C. and Chen, T., 2021. Why pre-charge circuits are necessary in high-voltage systems. Texas Instruments Application Brief, SLVAFB0. https://www.ti.com/lit/ab/slvafb0/slvafb0.pdf

[9] Paudel, S., Zhang, J., Ayalew, B., Griddaluru, V.Y. and Singh, R., 2025. Design, prototyping, and integration of battery modules for electric vehicles and energy storage systems. Electricity, 6(4), p.63. https://doi.org/10.3390/electricity6040063

[10] Kharanaq, F.A., Emadi, A. and Bilgin, B., 2020. Modeling of conducted emissions for EMI analysis of power converters: State-of-the-art review. IEEE Access, 8, pp.189313–189325. https://doi.org/10.1109/ACCESS.2020.3031693